

Ultrasonic Attenuation in Magnetic Single Crystals*

SHELDON LEVY AND ROHN TRUELL

Brown University, Providence, Rhode Island

A striking connection has been found between the magnetic properties and the ultrasonic attenuation properties of a nickel single crystal. The magnetic anisotropy has been detected by measuring the attenuation as a function of applied field intensity. Information about the vibrations of Bloch walls and the number of vibrating walls per unit length has also been obtained. The dependence of the attenuation on magnetic induction for 5–100 mc shear and longitudinal waves propagated in the $[1\bar{1}0]$ direction was the same for B parallel to both the $[111]$ and $[001]$ directions. The shear modes induce much greater losses than the longitudinal mode.

Similar measurements on a 3.8 percent Si-Fe crystal showed that the walls in this alloy are not as easily vibrated, i.e., there is a small difference in attenuation between the magnetized and unmagnetized states. At these frequencies this indicates that there is a direct connection between the magnetostrictive constants and the dynamic behavior of Bloch walls.

The elastic constants were computed from velocity measurements, but no ΔE effect was observed.

Pulsed ultrasonic techniques as described by Roderick and Truell (see reference 4) were used in taking the measurements. The single crystals used were grown from the melt in a hydrogen atmosphere and then oriented so that pure modes of vibration could be propagated.

I. INTRODUCTION

IT is well known that internal strain is coupled to Bloch wall movement in a ferromagnetic material; however, no law governing the interaction has been established. This coupling is responsible for the magnetomechanical loss which occurs when an elastic wave traverses a ferromagnetic material.

Recently there has been a great deal of interest in the magnetomechanical losses^{1–3} as well as the absorption of ultrasound in the saturated crystal. This last interest is due to the possibility of using such measurements to determine ferromagnetic resonance.

It is about the magnetomechanical losses associated with the transmission of 5–100 mc ultrasound through Ni and 3.8 percent Si-Fe crystals that this paper is written.

II. EXPERIMENTAL METHODS

1. Ultrasound Equipment and Techniques

The pulsed ultrasound technique for determining attenuation and velocity in solids requires the production of a short pulse of mechanical energy and the ability to accurately measure the ratio of the amplitudes of successive echoes and the time-delays between them. At megacycle frequencies this can be done with radar type circuits and piezoelectric transducers which convert the electrical energy into mechanical energy and vice versa. Such equipment has been built in the Metals Research Laboratory at Brown University and has been described elsewhere.^{4,5} The transducers, X and AC -cut quartz, were cemented to the specimens with salol.

* Supported by the United States Air Force Contract AF 33(038)—15602.

¹ J. De Klerk, *Nature (London)* **168**, 963 (1951).

² Bozorth, Mason, and McSkimin, *Bell Syst. Tech. J.* **30**, 970 (1951).

³ T. F. Rogers and S. J. Johnson, *J. Appl. Phys.* **21**, 1067 (1950).

⁴ R. L. Roderick and R. Truell, *J. Appl. Phys.* **23**, 267–279 (1952).

2. Specimen Preparation

The large single crystals of nickel and 3.8 weight percent silicon-iron used were grown from the melt in a hydrogen atmosphere and then accurately oriented by means of x-rays. The stock metals from which they were grown had the following trade names and percent purities: Mond nickel pellets, 99.90; Plast-Iron, 99.91; silicon (Electrometallurgical Corporation), 99.8+.

Surfaces parallel to the (100), (010), and (011) planes were cut and accurately ground on both Si-Fe crystals while the nickel crystal was prepared with its surfaces parallel to the (111), $(1\bar{1}0)$, and (001) planes, as in Fig. 1. These planes were chosen to satisfy the requirements for propagating longitudinal and shear elastic waves in the crystal (see Appendix I) and permitted the external magnetic field to be applied in the easy, medium, and hard directions of magnetization in the nickel sample.

Great care was exercised in surface grinding the crystals so that the strained layer caused by this operation would be as shallow as possible. The depth of the layer in the nickel crystal was less than 0.1 mm as was determined by taking back reflection Laue photographs after successive acid etches until all strained material was shown to be removed. The sharply defined Laue spots on the last of the above photographs indicated that the crystal was well annealed and possessed a high degree of perfection.

The dimensions of the nickel crystal Ni-I are $l_{[1\bar{1}0]}$ = 1.28 cm, $l_{[001]}$ = 1.76 cm, and $l_{[111]}$ = 1.67 cm. The Fe-Si crystals will be referred to as Fe-Si I and Fe-Si II,

⁵ R. Roderick, Ph.D. thesis, "On the measurements of ultrasonic attenuation in solids by the pulse technique," Brown University (1951).

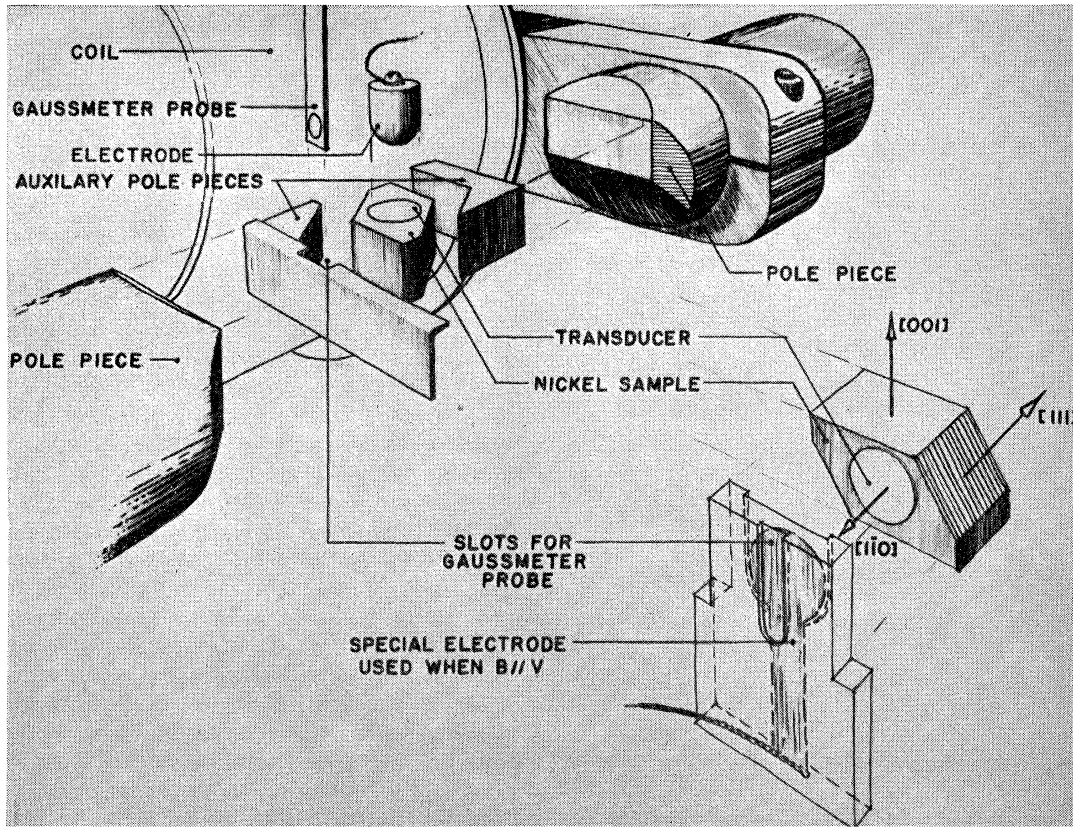


FIG. 1. Exploded view of experimental arrangement.

whose respective dimensions are $l_{[100]}=2.35$ cm, $l_{[011]}=1.29$ cm, and $l_{[100]}=2.28$ cm, $l_{[011]}=2.07$ cm.

3. Magnetic Considerations and Measurements

The magnetic field was supplied by an electromagnet with a cold-rolled steel core of 16 cm² mean area, wound with 5550 turns of No. 22 wire. The cylindrical poles of the magnet were tapered to a rectangular shape 1.6 cm \times 3.2 cm, which permitted a uniform field of 19 kilogauss to be obtained with an air gap of 0.1 cm.

Because of the irregular shape of the nickel crystal and its large anisotropy energy, auxiliary soft iron pole pieces (accurately ground to match the crystal surfaces) were inserted when the magnetic field was applied in the [001] and [111] directions. These were essential when the field was applied in the hard direction of magnetization because of the large anisotropy energy.

The magnetic field was measured with a Dyna-Labs Gaussmeter (probe size 1.75 in. \times 0.200 in. \times 0.025 in.), which measures the component of magnetic induction normal to a germanium crystal whose cross-sectional area is 0.01 in.². The probe was inserted in the air gap between the auxiliary pole pieces and the specimen, and it was assumed that the field measured was the same as the field in the specimen. This assumption was made because the normal component of the induction must be continuous across a boundary. The accuracy of the gaussmeter was within 3 percent as determined by

measuring the field of a solenoid and was frequently checked with a 1000-gauss standard.

When the field was applied parallel to the direction of propagation, a special electrode was used.

Figure 1 shows the arrangement employed for applying and measuring the magnetic field.

III. EXPERIMENTAL RESULTS

1. Velocity Measurements

The velocity of propagation of ultrasound in nickel was measured at 27 mc for a longitudinal wave propagated in the [001] direction and at 30 mc for the longitudinal and the two transverse waves propagated in the $[\bar{1}10]$ direction. The mean time delay between echoes was obtained by least square computations, and the effect of the transducer on the length of the sound path was not taken into account. These velocities and the elastic parameters as computed from (11) and (13) of the Appendix I and $\rho=8.90$ g/cm³ are listed below:

$$\begin{aligned} V_{[100]} &= 5.27 \times 10^5 \text{ cm/sec,} \\ V_{[110]} &= 5.96 \times 10^5 \text{ cm/sec,} \\ V_{T_{2[110]}} &= 3.69 \times 10^5 \text{ cm/sec,} \\ V_{T_{1[110]}} &= 2.31 \times 10^5 \text{ cm/sec,} \\ C_{11} &= 2.47 \times 10^{12} \text{ dynes/cm}^2, \\ C_{44} &= 1.21 \times 10^{12} \text{ dynes/cm}^2, \\ C_{12} &= 1.52 \times 10^{12} \text{ dynes/cm}^2. \end{aligned}$$

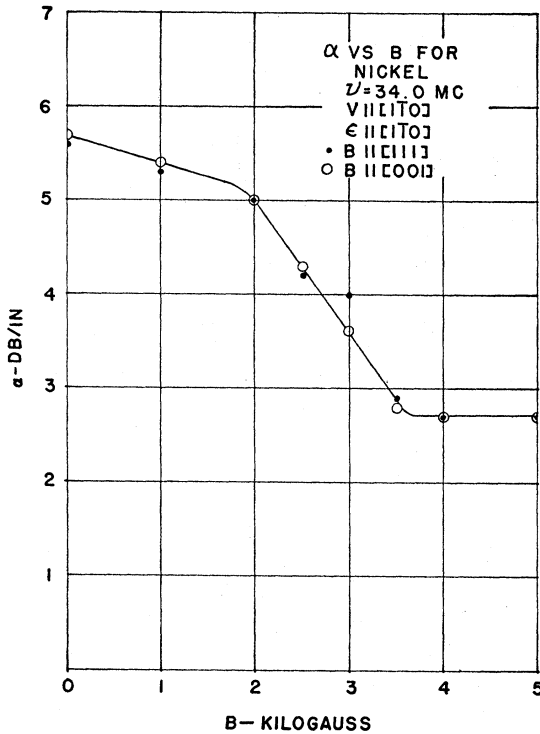


FIG. 2. Attenuation vs induction for Ni showing coincident behavior for B parallel to the easy and hard directions of magnetizations.

The ΔE effect was not observed at any frequency covered, i.e., no change in velocity with the application of a magnetic field was detected.

The velocities of propagation of ultrasound in 3.8 percent Si-Fe, and the corresponding elastic parameters were found to be

$$\begin{aligned} V_{[100]} &= 5.30 \times 10^5 \text{ cm/sec,} \\ V_{[110]} &= 6.20 \times 10^5 \text{ cm/sec,} \\ V_{T[100]} &= 4.01 \times 10^5 \text{ cm/sec,} \\ C_{11} &= 2.15 \times 10^{12} \text{ dynes/cm}^2, \\ C_{12} &= 1.27 \times 10^{12} \text{ dynes/cm}^2, \\ C_{44} &= 1.23 \times 10^{12} \text{ dynes/cm}^2. \end{aligned}$$

In computing the above we used $\rho = 7.65 \text{ g/cm}^3$.

2. Dependence of the Attenuation of Ultrasound in Nickel on the Magnetic Induction

The attenuation per unit length was computed using the method of least squares from measurements taken with the techniques described in Part II. In all cases only readings taken within the plane wave region were used.⁴ Except for frequencies adjacent to 50 mc the measurements were highly reproducible if care was taken in cementing the transducer to the sample. In fact, measurements taken at the same frequency obtained by using different harmonics of separate transducers (e.g., ninth of 5.5 mc and seventh of 7.0 mc)

gave attenuation measurements well within experimental error.

The results for the case $V \parallel [1\bar{1}0]$, $\epsilon \parallel [1\bar{1}0]$ are shown in Figs. 2, 3, 4, and 5. The coincident dependence of the attenuation coefficient α , in $DB/in.$, on the induction for an ultrasonic wave with $V \parallel [110]$, $\epsilon \parallel [1\bar{1}0]$ when the induction is in the easy or hard directions of magnetization, is shown by Fig. 2, which is representative of these plots at all frequencies.

A composite graph showing the relation between α and B at 5.8, 16.5, 21, 27, 30, 52, and 90 mc for $V \parallel [1\bar{1}0]$, $\epsilon \parallel [1\bar{1}0]$, and $B \perp V$ is given by Fig. 3. The sharp break at the "knee" and "instep" of the curves was easily observed when the measurements were made and occurred at 1800 and 3800 gauss for all frequencies.

The variation of the attenuation with frequency is shown in Fig. 4, where the attenuation coefficient for zero and saturation values of induction are plotted. A "dip" in both curves occurred near 49 mc and was first thought to be due to the low frequency equipment. This opinion was not substantiated, however, for later the dip occurred in measurements made with the high frequency gear and was then attributed to a "resonance" in the nickel. Later the source of the dip become even more difficult to explain when an indication of this effect was observed at 49 mc for transverse waves (cf. Fig. 7), whose wavelength differed by nearly a factor of two. Figure 5 shows the dependence of α on B for $V \parallel [110]$, $\epsilon \parallel [1\bar{1}0]$, and $B \parallel [1\bar{1}0]$ at 15, 19.5, and 34.5 mc. Here the sharpness of the "knee" and "instep"

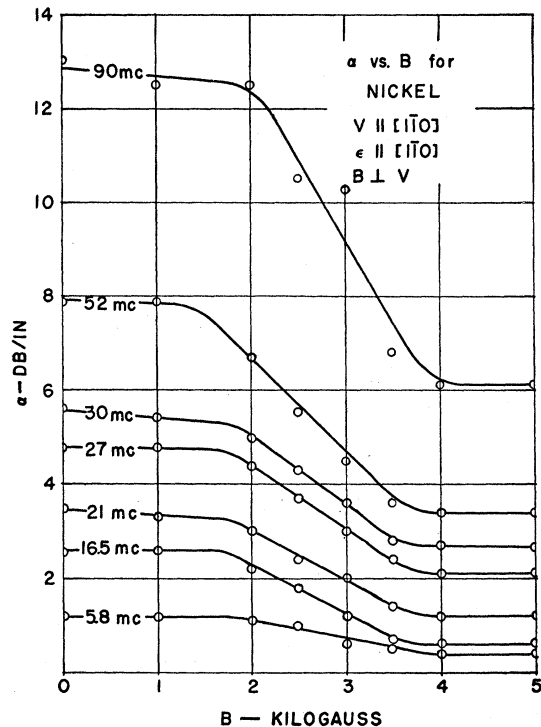


FIG. 3. Attenuation vs induction for Ni with $V \parallel [1\bar{1}0]$, $\epsilon \parallel [1\bar{1}0]$, and $B \perp V$ at 5.8, 16.5, 21, 27, 30, 52, and 90 mc.

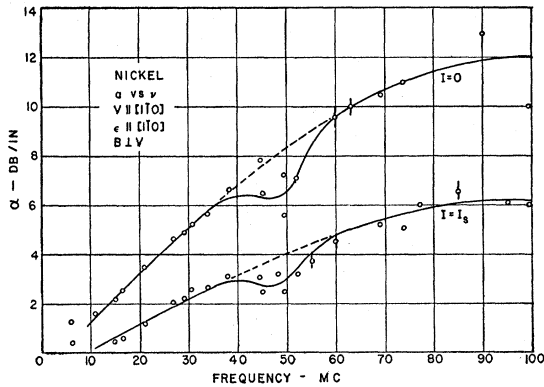


FIG. 4. Attenuation vs frequency for Ni in the unmagnetized state ($I=0$) and saturated state ($I=I_s$) with $V||[110]$, $\epsilon||[110]$, and $B \perp V$.

breaks is absent, but the value of α for zero and saturation induction is in agreement with the values obtained for $B \perp V$.

The coincident behavior of α vs B for the two possible cases of $B \perp V$ was observed at all frequencies used for $V||[1\bar{1}0]$ and $\epsilon||[001]$.

A composite plot of α vs B for $V||[1\bar{1}0]$, $\epsilon||[001]$, and $B \perp V$ is shown in Fig. 6, while Fig. 7 reveals the dependence of α (saturation) and α (no field) on frequency for these conditions.

Only one set of measurements was taken with $V||[1\bar{1}0]$, $\epsilon||[110]$, and $B \perp V$. The response of α to the induction for this case at 10 mc is shown in Fig. 8.

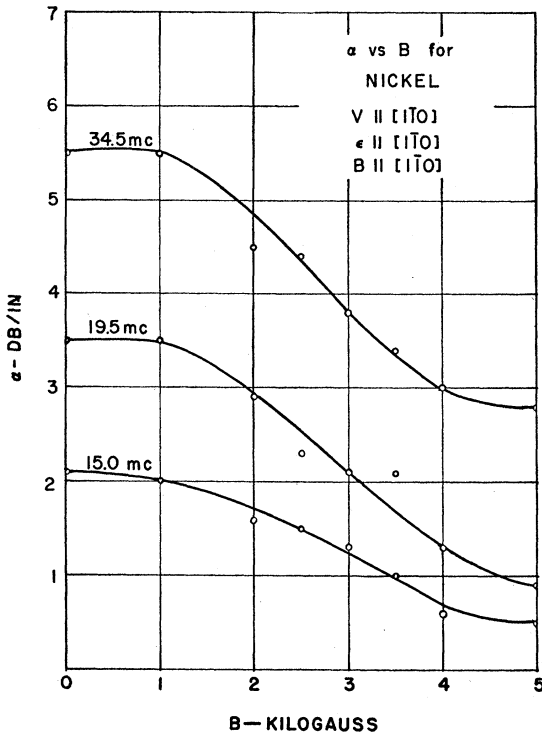


FIG. 5. Attenuation vs induction for Ni with $V||[1\bar{1}0]$, $\epsilon||[1\bar{1}0]$, and $B||V$ at 15, 19.5, and 34.5 mc.

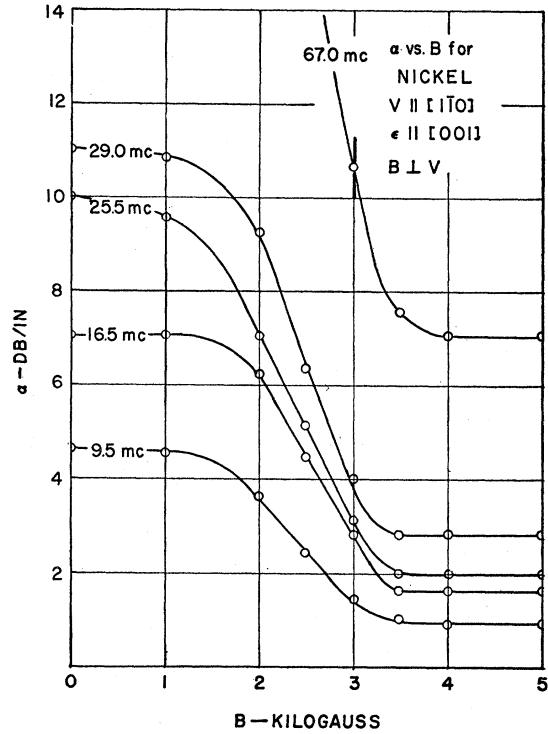


FIG. 6. Attenuation vs induction for Ni with $V||[1\bar{1}0]$, $\epsilon||[001]$, and $B \perp V$ at 9.5, 16.5, 25.5, and 29 mc.

The coincident dependence of α and B for $B \perp V$ in the foregoing results is further exemplified by Fig. 9 where the attenuation coefficient for a transverse wave is plotted against the magnetization current. This current is essentially proportional to the magnetic field intensity H . These measurements show the behavior one would expect from the foregoing results on the dependence of α on B and the $B-H$ curves for the easy and hard directions of magnetization of nickel.

The attenuation coefficient of 3.8 percent Si-Fe was found to be small at all frequencies, less than 1 DB/in. at 50 mc for longitudinal vibrations in the $[110]$ direction. The change in this value as a saturation

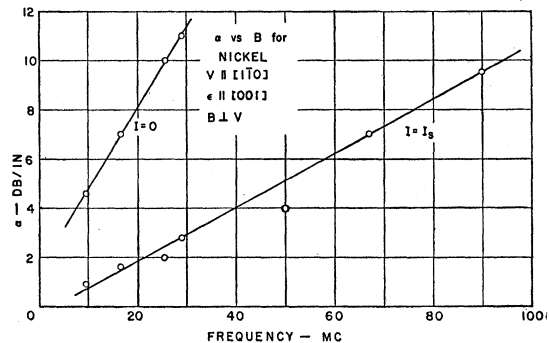


FIG. 7. Attenuation vs frequency for Ni in the unmagnetized state ($I=0$) and saturated state ($I=I_s$) with $V||[1\bar{1}0]$, $\epsilon||[001]$, and $B \perp V$.

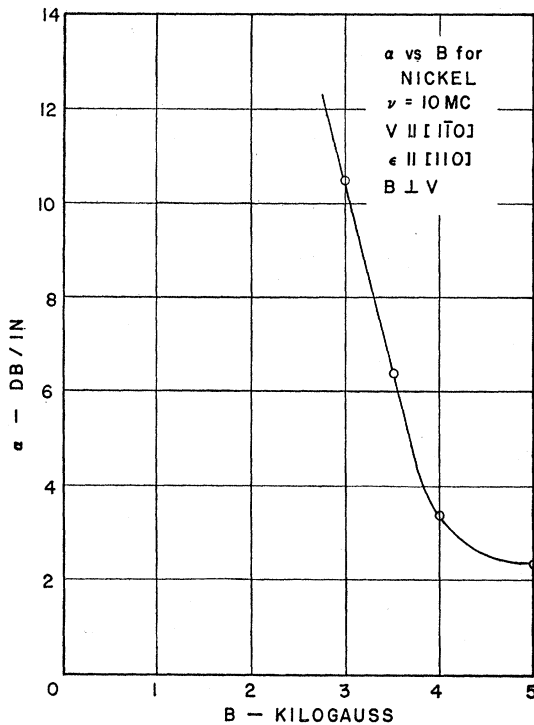


FIG. 8. Attenuation vs frequency for Ni with $V \parallel [1\bar{1}0]$, $\epsilon \parallel [110]$, and $B \perp V$ at 10 mc.

magnetic field was applied, and although present, was not measurable with the present equipment.

IV. CONCLUSION

The magnetomechanical losses associated with the propagation of ultrasound through a nonsaturated ferromagnetic crystal arise from the fact that the spins of the lattice are affected by the energy in the sonic wave. While the law governing the behavior of the spins as the elastic wave traverses them has not been established, it is plausible to consider the Bloch wall as being "driven" by the harmonic elastic wave. Two effects probably occur: (1) a vibration of the center plane of the wall, and (2) a periodic variation in the width of the wall. A combination of these two effects include domain rotations.

An extension of theoretical calculations by one of the authors[†] has shown that the magnetomechanical losses, to a first-order approximation, are the result of "rigid wall" vibrations. This work led to defining a "coupling coefficient," k , which relates the amplitude of the wall vibration to the energy in the ultrasonic beam. Furthermore, the calculations showed the attenuation due to magnetomechanical effects is proportional to the number of domain walls affected by the ultrasonic wave.

The theory agrees, in principle, with the experimental results as interpreted from the shape of the attenuation coefficient α versus magnetic induction B curves, which exhibit no magnetic anisotropy.

[†] S. L. Levy, Ph.D. thesis, Brown University, 1952.

In the approximate ranges $0 < B < \frac{1}{3}B_s$, $\frac{1}{3}B_s < B < \frac{2}{3}B_s$, and $\frac{2}{3}B_s < B$ one has small decrease in α , large linear decreases in α and constant α , respectively, as B increases.

The first of these ranges corresponds to reversible wall movements and show that k decreases slightly with increasing induction. For $\frac{1}{3}B_s < B < \frac{2}{3}B_s$ there are reversals of the domains resulting in a loss of the number of domain walls. The experimental results in this range indicate a linear decrease in the number of movable domain walls per unit length with increasing B .

A proposed explanation for the constant value of α when $B > \frac{2}{3}B_s$ is that walls with some orientations, because of the anisotropy, may not be affected by the ultrasonic wave. Hence, after $B \approx \frac{2}{3}B_s$, all of the walls which can be vibrated by the wave have been eliminated in the magnetization process. We speak here of wall motion in the general sense which includes partial rotation of the domain.

The smoothing out of the curves (Fig. 5) as compared with Fig. 3) showing the response of α vs B for $B \parallel V \parallel \epsilon \parallel [1\bar{1}0]$ may have been caused by the larger air gap required in the magnetic circuit in order that the special electrode (Fig. 1) could be inserted. This effect warrants further investigation.

As expected, greater sensitivity occurred when transverse waves were used. The anisotropy or the large difference of attenuation between the two polarizations of transverse waves propagated in the $[1\bar{1}0]$ direction is interesting. The attenuation was so great in the unmagnetized state for $V \parallel [1\bar{1}0]$ and $\epsilon \parallel [110]$ that no echoes were observable at 10 mc. However, by extrapolating the data taken near the saturation region one finds that the attenuation caused by magnetomechanical losses is approximately 30–35 db/in. which agrees with Bozorth, Mason, and McSkimin's² value of 32 db/in.

The results of the experiments reported here indicate that k is frequency dependent, large for highly magnetostrictive materials, and small for those materials which exhibit little magnetostriction.

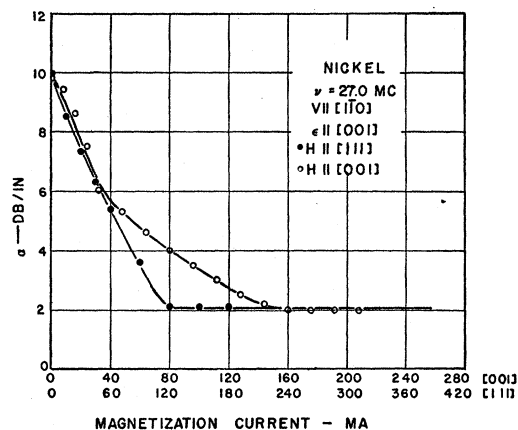


FIG. 9. Anisotropy of attenuation in Ni at 27 mc with $V \parallel [1\bar{1}0]$, $\epsilon \parallel [001]$.

The ease with which the elastic parameters can be determined with pulsed ultrasound is apparent from (11) and (13) of Appendix I. The values obtained for the elastic parameters of nickel agree with those reported in the literature.^{2,3,5-7}

ACKNOWLEDGMENT

The suggestions of Mr. H. J. Williams of the Bell Telephone Laboratories on the processing of single crystals are gratefully acknowledged as are the contributions of the staff of the Metals Research Laboratory at Brown University. Accurate orientation of the crystals was made possible by the generous loan of a 90° Norelco Geiger Counter Spectrometer by the M. W. Kellogg Corporation.

APPENDIX I. ON THE PROPAGATION OF LONGITUDINAL AND TRANSVERSE WAVES IN AN ANISOTROPIC ELASTIC SOLID

In an anisotropic elastic solid the stress-strain relations are

$$\sigma_{ij} = c_{ijkl} e_{kl} \quad i, j = 1, 2, 3, \quad (\text{A1})$$

where the c_{ijkl} are the elastic parameters. In the absence of body forces the equations of equilibrium read

$$\sigma_{ij,i} = \rho \ddot{u}_j, \quad j = 1, 2, 3. \quad (\text{A2})$$

Here ρ is the density of the solid. Using the definition of the strain $\epsilon_{ij} = \frac{1}{2}(\dot{u}_{i,j} + u_{j,i})$, one gets from (A1) and (A2)

$$\frac{1}{2} c_{ijkl} (u_{k,i} + u_{l,j}) = \rho \ddot{u}_j, \quad j = 1, 2, 3. \quad (\text{A3})$$

If a plane wave is traveling in the (l_1, l_2, l_3) direction with the velocity v and the displacement is in the (d_1, d_2, d_3) direction, one has the displacements given by

$$u_j = A d_j e^{i\kappa(vt - l \cdot r)} \quad j = 1, 2, 3, \quad (\text{A4})$$

where κ is propagation constant. The l_i 's, d_i 's, and v must satisfy

$$c_{ijkl} l_j l_k d_l = \rho v^2 d_j, \quad j = 1, 2, 3. \quad (\text{A5})$$

For any direction of propagation (A5) gives three real velocities (see Love⁹), which have mutually orthogonal displacements.

For cubic symmetry (1) has the form

$$\begin{aligned} (c_{11} - c_{44}) l_1^2 d_1 + (c_{12} + c_{44}) l_1 l_2 d_2 + (c_{12} + c_{44}) l_1 l_3 d_3 &= (\rho v^2 - c_{44}) d_1, \\ (c_{12} + c_{44}) l_2 l_1 d_1 + (c_{11} - c_{44}) l_2^2 d_2 + (c_{12} + c_{44}) l_2 l_3 d_3 &= (\rho v^2 - c_{44}) d_2, \\ (c_{12} + c_{44}) l_3 l_1 d_1 + (c_{12} + c_{44}) l_3 l_2 d_2 + (c_{11} - c_{44}) l_3^2 d_3 &= (\rho v^2 - c_{44}) d_3, \end{aligned} \quad (\text{A6})$$

⁶ K. Honda, and Y. Shirakawa, Sci. Rep. Res. Inst. Tohoku Univ. 1, 9 (1949).

⁷ M. Yamamoto, Phys. Rev. 77, 566 (1950).

⁸ Bozorth, Mason, McSkimin, and Walker, Phys. Rev. 75, 1954 (1949).

⁹ A. E. H. Love, *Mathematical Theory of Elasticity* (Cambridge University Press, 1934), fourth edition, p. 298.

where

$$\begin{aligned} c_{11} &= c_{1111} = c_{2222} = c_{3333}, \\ c_{12} &= c_{1122} = c_{2211} = c_{1133} = c_{3311} = c_{2233} = c_{3322}, \\ c_{44} &= c_{1212} = c_{2121} = c_{1313} = c_{3131} = c_{2323} = c_{3232}, \\ 0 &= c_{ijkl} \text{ for all other parameters.} \end{aligned} \quad (\text{A7})$$

Solving (A6) for the displacement direction, one obtains

$$(d_1, d_2, d_3) = \left(\frac{l_1}{\lambda + c l_1^2}, \frac{l_2}{\lambda + c l_2^2}, \frac{l_3}{\lambda + c l_3^2} \right). \quad (\text{A8})$$

Here $\lambda = \rho v^2 c_{44}^{-1} - 1$ and $c = (c_{12} + 2c_{44} - c_{11}) c_{44}^{-1}$ is the anisotropy factor.

In ultrasonic testing one usually uses either longitudinal or transverse waves; hence we shall consider these modes of vibrations.

Case I. Longitudinal Waves

Equation (A8) gives

$$d_1 : d_2 : d_3 = \frac{l_1}{\lambda + c l_1^2} : \frac{l_2}{\lambda + c l_2^2} : \frac{l_3}{\lambda + c l_3^2}. \quad (\text{A9})$$

If $c \neq 0$, clearly

$$\begin{aligned} l_1 &= l_2 = l_3, \\ l_1 &= l_2, \quad l_3 = 0, \\ l_1 &\neq 0, \quad l_2 = l_3 = 0, \end{aligned} \quad (\text{A10})$$

and their equivalents are the only directions in which longitudinal waves can be propagated. From (A6) one finds the corresponding ρv 's are

$$\begin{aligned} \rho v^2 T_{[100]} &= c_{11}, \quad \rho v^2 T_{[110]} = \frac{1}{2}(c_{11} + c_{12} + 2c_{44}), \\ \rho v^2 T_{[111]} &= \frac{1}{3}(c_{11} + 2c_{12} + 4c_{44}). \end{aligned} \quad (\text{A11})$$

Case II. Transverse Waves

From (A8) and $d_i l_i = 0$ one gets

$$\lambda^2 + 2\lambda c(l_1^2 l_2^2 + l_2^2 l_3^2 + l_3^2 l_1^2) + c^2 l_1^2 l_2^2 l_3^2 = 0. \quad (\text{A12})$$

If the solutions for λ of (A12) are substituted into (A6), one finds that the only directions which satisfy the conditions for transverse waves are those which satisfy the conditions for longitudinal waves. Furthermore, it is only necessary to polarize the vibration for propagation in the [110] direction. The ρv 's are

$$\begin{aligned} \rho v^2 T_{[100]} &= c_{44}, \\ \rho v^2 T_{[110]} &= c_{44}, \\ \rho v^2 T_{[111]} &= \frac{1}{2}(c_{11} - c_{12}), \\ \rho v^2 T_{[111]} &= \frac{1}{3}(c_{11} + c_{44} - c_{12}). \end{aligned} \quad (\text{A13})$$

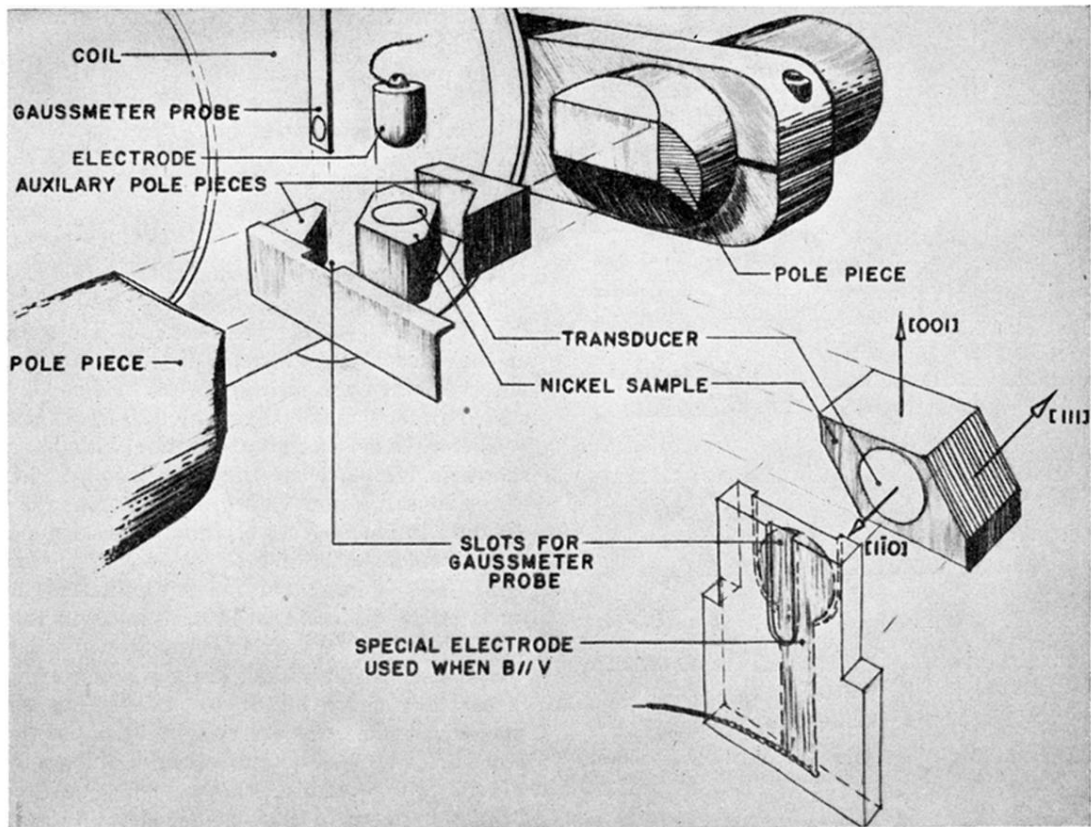


FIG. 1. Exploded view of experimental arrangement.